Available online at www.sciencedirect.com
ScienceDirect
Journal of the European Ceramic Society 31 (2011) 3127–3135
www.elsevier.com/locate/jeurceramsoc

Growth of 20 mol% Gd-doped ceria thin films by RF reactive sputtering: The O_2/Ar flow ratio effect

Yu-Lin Kuo [a,*], Yong-Siou Chen [b], Chiapyng Lee [b]

[a] Department of Mechanical Engineering, National Taiwan University of Science and Technology, No. 43, Section 4, Keelung Road, Taipei 10607, Taiwan
[b] Department of Chemical Engineering, National Taiwan University of Science and Technology, No. 43, Section 4, Keelung Road, Taipei 10607, Taiwan

Available online 24 May 2011

Abstract

The search for optimal materials and the utilization of proper manufacturing techniques to replace conventional electrolytes are our research objectives for the operation of solid oxide fuel cells under intermediate temperatures. Furthermore, understanding the effects of process parameters will be helpful for obtaining suitable materials for applications. In this study, we investigate the O_2/Ar flow ratio effect by employing RF reactive sputtering to fabricate 20 mol% Gd-doped ceria (20GDC) films on alumina substrates. The morphology of films was aggregated by nano-scale size of grains which gradually reduced in size from lower to higher O_2/Ar flow ratios. The microstructure of films was transferred from incomplete oxidized materials to well-crystallized cubic fluorite structures using an increased O_2/Ar flow ratio up to 0.30. The oxygen/metal ratio of films was increased gradually and saturated around 2.05 for O_2/Ar flow ratios over 0.25 and remained in uniform composition through whole films for each flow ratios.

Keywords: CeO_2; A. Films; C. Chemical properties; B. Spectroscopy; Fuel cells

1. Introduction

Ceria based ceramics have been studied for several decades due to their usefulness in transferring oxygen ions through its cubic fluorite structure. The applications of ceria based materials can resemble something akin to a catalytic converter or operate as a metal support material in a wide range fields. The ability to transfer oxygen ions from its structure is described by the principles of ionic conductivity; this ability to transfer can be further enhanced by creating excess oxygen vacancies within its lattice structure via adding a suitable amount of divalent alkaline earth ions (e.g., Ca^{2+} and Sr^{2+}) or trivalent rare earth ions (e.g., Y^{3+}, La^{3+}, Gd^{3+}, and Sm^{3+}) to replace its cation sites.[1–3]

In the field of solid oxide fuel cells (SOFCs), current research tends to focus on Gd^{3+} or Sm^{3+} doped ceria as an alternative to solid electrolytes due to its more effective conductivity as compared to traditional zironia based materials in the intermediate temperature range (500–700 °C).[4] The advantages of reducing the operating temperature include not only widening the range of materials choices for anode, cathode and interconnector components of fuel cell, but the process also serves to alleviate several substantial issues prone to take place between the solid electrolyte and electrodes such as cracking, coking, and aging during fuel cell operation.

Although the noble properties of ceria based materials can be obtained by adjusting the material structure itself, a comparable fabrication technique is still required to achieve an efficient SOFCs system. The voltage loss from the electrolyte material during the SOFCs operation is defined as ohmic polarization. Based on the fundamental of electrochemistry, the extent of ohmic polarization is inversely proportional to the thickness of electrolyte, meaning that voltage loss during fuel cell operation can be greatly reduced by decreasing the layer thickness of electrolyte.[5] As a result, developing a proper thin film preparation technique to improve the performance of SOFCs is required.

In the literature, several thin film preparation methods have been proposed, such as: chemical vapor deposition (CVD),[6,7] E-beam,[8] sputtering,[9–13] and spray pyrolysis.[14] Of these methods, the sputtering technique presents itself as the best candidate for preparing the solid electrolyte material as it has been to shown to be a reliable process for thin film deposition. This technique is commonly utilized in the semiconductor industry to fabricate a thin, dense, uniform layer on either a flat or porous substrate; this

* Corresponding author. Tel.: +886 2 27376784; fax: +886 2 27376460.
E-mail addresses: ylkuo@mail.ntust.edu.tw (Y.-L. Kuo), M9506006@mail.ntust.edu.tw (Y.-S. Chen), cplee@mail.ntust.edu.tw (C. Lee).

0955-2219/$ – see front matter © 2011 Elsevier Ltd. All rights reserved.
doi:10.1016/j.jeurceramsoc.2011.05.002

technique can also be used to fabricate a thin film SOFC system on a large commercialized scale. In addition, the high sintering temperature is not required during the sample preparation process as compared to the conventional preparation methods which allows it to avoid possible interfacial reactions between the electrode and electrolyte.

In fabricating a sputtered electrolyte thin film, the deposition parameters are strongly influenced by the surface morphology, crystal structure, and the chemical composition of the electrolyte materials. However, these materials properties are also correlated with the ionic conductivities of electrolyte materials, arguing the importance of discovering the relationship between the deposition parameters and the material properties of the sputtered electrolyte materials.

In this study, we focus on investigating the material characteristics of GDC films prepared by a RF reactive magnetron sputtering from a Ce–20 at% Gd alloy target in a serious set of O_2/Ar gas mixtures. The different O_2/Ar gas mixtures provide a distinct redox environment for each GDC film during preparation. The film's texture, crystallite size, microstructure, and composition were strongly correlated with the O_2/Ar flow ratios and were systematically examined using SEM, XRD and XPS.

2. Experimental procedure

2.1. Sample preparation

The substrate used in this study was a non-polished alumina plate with a thickness of 0.6 mm. Before loading into the sputtering chamber, the substrates were cut into a suitable size and ultrasonically cleaned in acetone and de-ionized water for 15 min, respectively. This was followed by drying in a stream of highly purified nitrogen gases for each experiment. The 20GDC films were prepared using RF-sputtering by means of a Ce–20 at% Gd (99.995% in purity) alloy target (3 in. diameter) at different O_2/Ar flow ratios. The base pressure (1.0×10^{-7} torr) was achieved by a diffusion pump. Prior to starting the deposition, the target was pre-sputtered in the argon gases (99.9995% in purity) for 10 min to ensure that pure Ce–20 at% Gd alloy surfaces were obtained.

During the deposition, the RF power supplied to the target was maintained at 200 W and hold at a target-to-substrate distance of 7.5 cm. A serious set of O_2/Ar flow ratios were achieved by varying the oxygen (99.999% in purity) flow rate to 0.5, 1.0, 1.5, 2.0, 2.5, 3.0, and 3.5 sccm with fixed argon flow rate (10 sccm). The total pressure was controlled at 8.5 mTorr by a throttle valve for each specific O_2/Ar flow ratio. The deposition time was constrained to 18 min for each 20GDC film preparation.

2.2. Material characterization and chemical composition

The surface morphology of the 20GDC films was examined by field emission scanning electron microscopy (FESEM). A JEOL JSM-6500F FESEM was used to examine samples which were prepared in both a plane-view and cross-sectional view. A Rigaku RTP 300 X-ray diffractometer was used to examine the crystalline structure of the films (Cu Kα radiation of $\lambda = 1.5405$ Å). Chemical bindings and composition of thin films were investigated using X-ray photoelectron spectroscopy (XPS). XPS was performed in a Thermo VG Scientific Sigma Probe spectrometer. All XPS data presented herein were acquired using a monochromatized Al Kα line (1486.6 eV) and were recorded at a constant pass energy of 50 eV with a resolution of 0.5 eV. Peak positions were then calibrated with respect to the C 1s peak at 284.5 eV from adventitious hydrocarbon contamination.

The data processing for XPS spectra in this study were resolved through background subtraction using the Shirley–Sherwood method and then deconvoluted in the Gaussian–Lorentzian components for each peak using Thermo Avantage XPS software. The energy doublet separation of partially reduced Ce $3d_{5/2}$–Ce $3d_{3/2}$, mainly reduced ceria Ce $3d_{5/2}$–Ce $3d_{3/2}$ and Gd $4d_{5/2}$–Gd $4d_{3/2}$ was constrained to 18.4, [15,16] 18.2[16] and 5 eV,[17,18] respectively. The intensity for each doublet peak was also fixed to 3:2 for $d_{5/2}$:$d_{3/2}$.[19]

From reviewing the study of XPS analysis on the ceria system, the oxidation state of cerium was easily affected by subjecting the samples to Ar^+ sputtering.[20,21] Therefore, all the XPS spectra described in this study were obtained without first cleaning with Ar^+ sputtering to avoid the risk of generating reduced ceria in the spectra and influencing the accuracy of data analysis as regards the oxidation state of cerium in the 20GDC films.

3. Results and discussion

The 20GDC films were prepared through RF reactive sputtering from a Ce–20 at.% Gd alloy target at various O_2/Ar

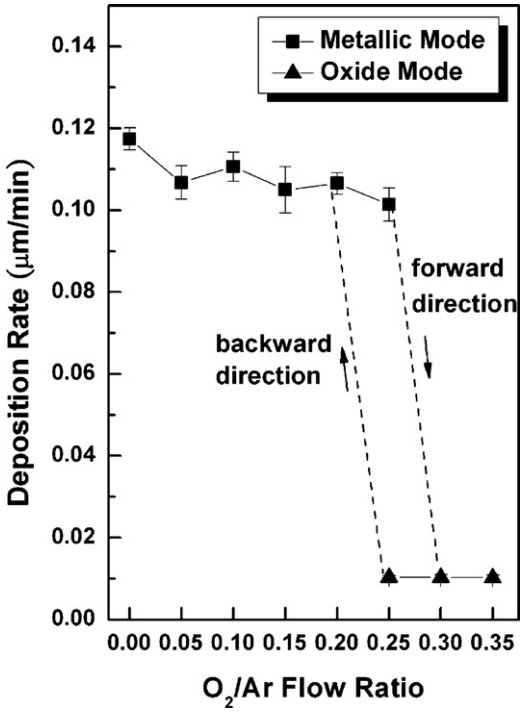

Fig. 1. Dependence of the deposition rate of 20GDC films as a function of O_2/Ar flow ratios.

flow ratios. During the sputtering deposition, the metallic target was subjected to consecutive etching and oxidizing procedures using the O_2/Ar gas mixture atmosphere. The chemical environment was specific to the deposition conditions of 20GDC films prepared at different O_2/Ar flow ratios. The deposition rate, surface morphology, crystal structure, and chemical composition of 20GDC films was strongly correlated with the O_2/Ar flow ratios during the sputtering deposition; this revealed a distinct material property for each of the 20GDC films prepared at different O_2/Ar flow ratios.

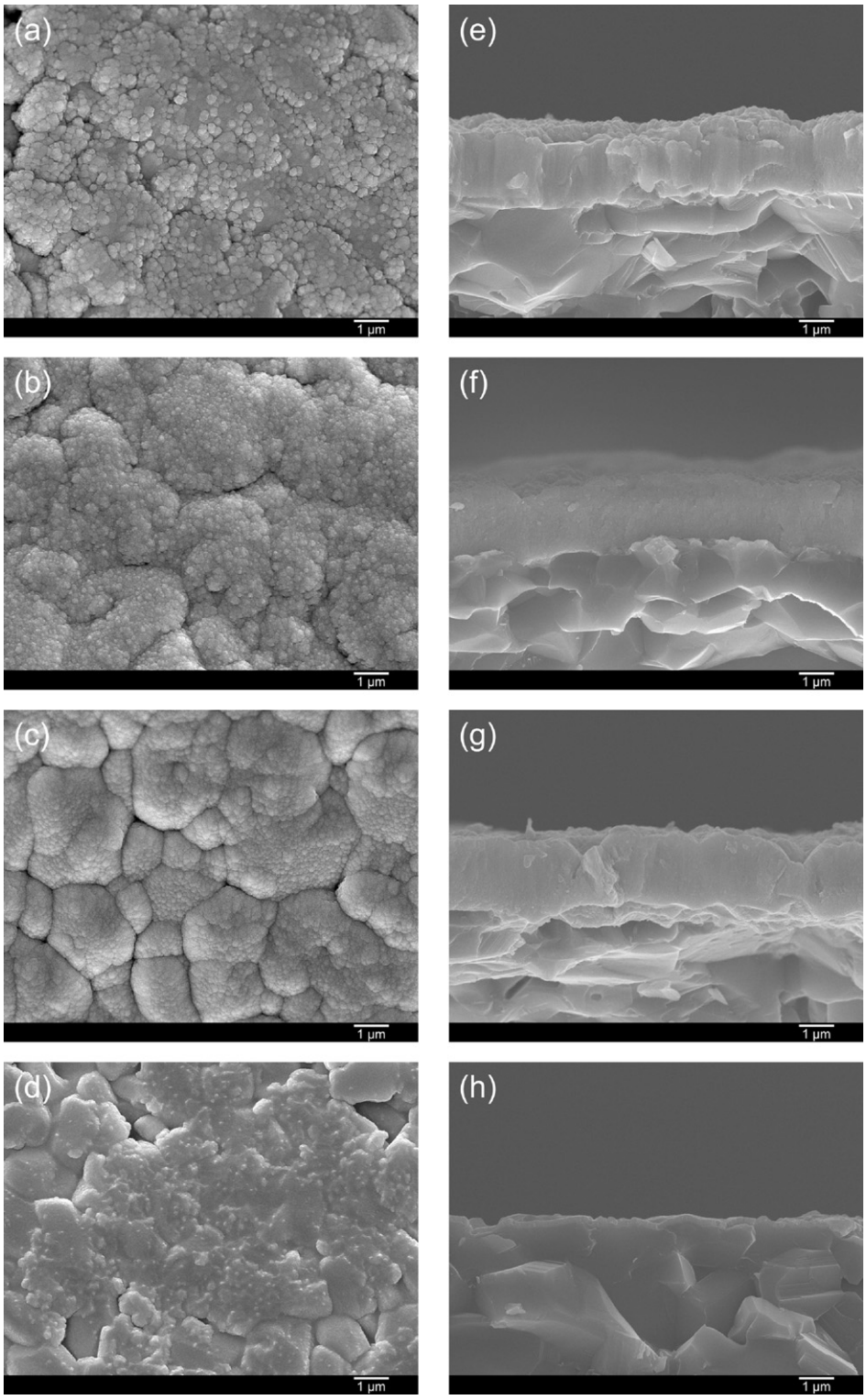

Fig. 2. SEM images of 20GDC films deposited at various O_2/Ar flow ratios: planar-view images (a) 0.05, (b) 0.20, (c) 0.25 in the metallic mode, (d) 0.25 in the oxide mode; cross-section view images (e) 0.05, (f) 0.20, (g) 0.25 in the metallic mode, (h) 0.25 in the oxide mode.

3.1. Effect of deposition rate

Fig. 1 shows the deposition rate of 20GDC films prepared at various O_2/Ar flow ratios. As can be seen from this figure, the profile of the deposition rate of 20GDC films was different as the experiment procedures progressed from a lower to higher O_2/Ar flow ratio (forward direction) or from a higher to lower O_2/Ar flow ratio (backward direction). In the forward direction, the deposition rate of 20GDC films was obtained around 0.10 μm/min as the O_2/Ar flow ratio was lower than 0.25, and encountered an abrupt drop to 0.01 μm/min as the O_2/Ar flow ratio rose above 0.30. It then remained a constant value while further increasing the O_2/Ar flow ratio. A similar result can also be obtained as the 20GDC films were deposited in the reverse direction. The only difference between these two directions was such that the deposition rate at the O_2/Ar flow ratio of 0.25 was much lower in the reverse direction as compared with the forward direction.

This characteristic phenomenon reveals a transition point which remains in two kinds of sputtering mechanisms decided by the design of experiment.[9] The transition point at the O_2/Ar flow ratio of 0.25 corresponded to a critical oxygen partial pressure of 1.3×10^{-3} torr.[22] As the oxygen partial pressure fell below this transition point, the surface composition of target was mainly occupied by the metallic materials and the mechanism of sputtering with a higher sputter yield (higher deposition rate) could be recognized as the metallic mode. On the contrary, when increasing the oxygen partial pressure over the critical pressure, the surface composition of target was fully oxidized and was generally characterized by a lower sputter yield than the metals, resulting in what we refer to as oxide mode (target poisoned). These results embody the typical characteristics of the deposition rate for the reactive sputtering of oxide materials.[9,22]

3.2. Effect of surface morphology and grain size

Fig. 2 shows a series set of planar-view and cross-section view SEM images of 20GDC films deposited at O_2/Ar flow ratios of 0.05 (Fig. 2a and e), 0.20 (Fig. 2b and f), 0.25 in the metallic mode (Fig. 2c and g), and 0.25 in the oxide mode (Fig. 2d and h). The 20GDC films prepared using RF reactive sputtering resulted in a crack-free and void-free structure which can be observed from the brittle fracture surfaces for all deposition conditions. At the lower O_2/Ar flow ratio of 0.05, the microstructure of 20GDC films were assembled by a mass of aggregated grains on the surfaces. The cross-sectional image revealed that the 20GDC films were highly dense throughout the films and were accompanied by no columnar structures which were generally seen in the sputtering of YSZ and GDC materials in the literature.[10–12]

While further increasing the O_2/Ar flow ratios to a higher extent during the deposition, the microstructure of 20GDC films exhibited no distinct change in their surface morphology as the O_2/Ar flow ratios were set to 0.10 and 0.15 (not shown). For O_2/Ar flow ratios over 0.20, the surface morphology of 20GDC films displayed a much smoother surface, as shown in Fig. 2b and d, and possessed a substrate-like morphology especially as the O_2/Ar flow ratio approached 0.25 in the metallic mode. Contrarily, for the 20GDC films prepared at O_2/Ar flow ratio of 0.25 in the oxide mode region (Fig. 2d and h), the surface morphology displayed a similar result but with a substantially less thickness and kept the same microstructure when subjected to an increased O_2/Ar flow ratio over 0.30.

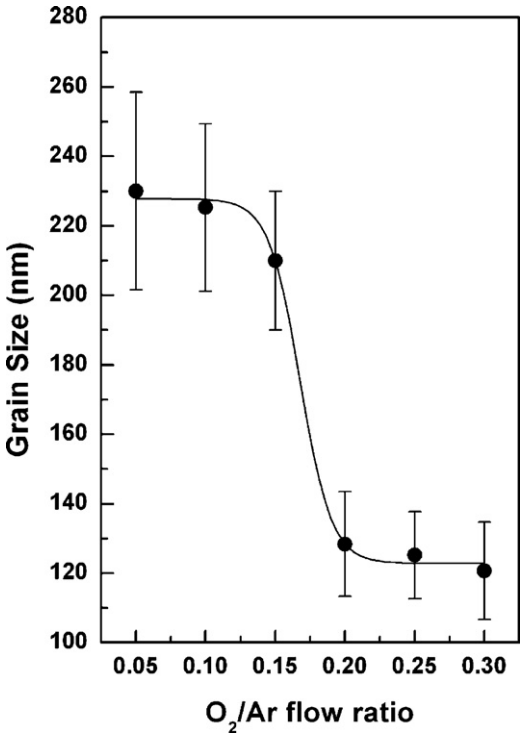

Fig. 3. Grain size of 20GDC films as a function of O_2/Ar flow ratio.

Fig. 3 shows the variation of grain size for 20GDC films measured from the planar-view SEM images at different O_2/Ar flow ratios. The grain size of 20GDC films gradually decreased with increased the O_2/Ar flow ratios. At the lower O_2/Ar flow ratios of 0.05, 0.10, and 0.15, the grain size of 20GDC films was around 220 ± 24 nm and then sharply decreased around 128 ± 14 nm for the higher O_2/Ar flow ratios over 0.20.

The variation of grain size and surface morphology of 20GDC films from the increased O_2/Ar flow ratios can be explained by examining the sputtering process during the films' deposition. In the typical reactive sputtering process, the ion-to-atom ratio of the sputtered materials from the metallic target was gradually increased by increasing the O_2/Ar flow ratio during film deposition. The higher adatom mobility and energy of the sputtered materials can be obtained for the higher O_2/Ar flow ratios. This results in higher diffusion energy of the sputtered materials on the surface of substrate for thin film deposition, and leads to a much smaller grain size and smoother surface morphology of 20GDC films for the O_2/Ar flow ratios over 0.20 in this study.[23,24]

3.3. Effect of crystal structure

Fig. 4 shows a typical set of XRD spectra for 20GDC films deposited at various O_2/Ar flow ratios in the wide-range scan

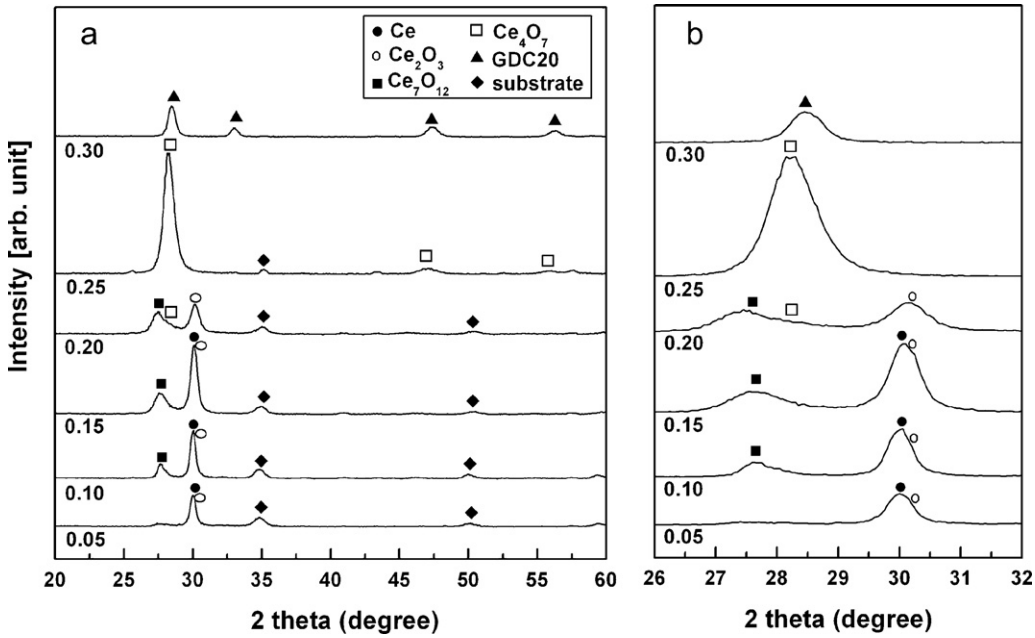

Fig. 4. XRD spectra of 20GDC films deposited at various O_2/Ar flow ratios (a) wide-range scan and (b) enlarged XRD spectra from 26° to 32° as denoted at (a).

from 20° to 60° and the enlarged XRD spectra from 26° to 32°. The XRD spectra suggested that the crystal structure of the 20GDC films held a mixing oxidation state of cerium materials when the O_2/Ar flow ratios were below 0.20 and transferred to a cubic fluorite structure of $Ce_{0.80}Gd_{0.20}O_{1.90}$ as the O_2/Ar flow ratio was raised to 0.30. However, since the diffraction intensities for the different mixing oxidation states of cerium materials in XRD spectra are somewhat weak and showed certain overlaid regions for different crystal structures, the structural information we referred here can only be speculated with XPS data which are discussed in Section 3.4.

In the wide-range scan using XRD, spectra, as shown in Fig. 4a, the crystal structure of 20GDC films deposited at an O_2/Ar flow ratio of 0.05 revealed two distinct diffraction patterns: one was the strongest peak belonging to the structure of Ce(1 1 1) at $2\theta = 30.00°$ from 20GDC films (marked as ●, JCPDS card 78-0638), the other was the structure of alumina (marked as ♦). However, during the examination of the enlarged XRD spectrum of 20GDC films in this flow ratio, a small shoulder of the diffraction peak of Ce(1 1 1) at $2\theta = 30.00°$ can be seen in Fig. 4b. After a comparison of the corresponding peak positions of Ce and Ce_2O_3 (marked as ○, JCPDS card 74-1145) in the JCPDS database, the results indicate that the strongest peak closed to 30.00° may include not only the signal of Ce(1 1 1) but also the contribution from Ce_2O_3(0 1 1). This particular mixing oxidation state of cerium materials for the as-deposited 20GDC films can be clearly resolved by the distinct shift of binding energy for the different valence state of cerium ions in the XPS spectrum, which is discussed in the next section.

Furthermore, while increasing the O_2/Ar flow ratio to 0.10, and subsequently 0.15, the intensity of the peak, which was close to 30.00°, became stronger. Additionally, the diffraction angles belonged to the structure of Ce_7O_{12}(0 0 3) and Ce_7O_{12}(2 1 1) (marked as ■, JCPDS card 71-0567), at $2\theta = 27.65°$ and 27.83°, were also accompanied with an increase of O_2/Ar flow ratio. This suggests that the 20GDC films were gradually oxidized by increasing the O_2/Ar flow ratio during sputtering deposition; this indicated that the increased intensity of the peak (close to 30.00°) was mainly caused by the increased amount of Ce_2O_3 materials in the films as the O_2/Ar flow ratio was raised to 0.10 and 0.15. Moreover, further increasing the O_2/Ar flow ratio to 0.20, the peak position was linked to the overlapped result of Ce(1 1 1) and Ce_2O_3(0 1 1) being shifted to the higher 2θ degree while the intensity of this peak was also reduced by the increase of O_2/Ar flow ratio. In addition, a broader shoulder at the higher 2θ degree of the peak belonging to Ce_7O_{12}(0 0 3) and Ce_7O_{12}(2 1 1) ($2\theta = 27.65°$ and 27.83°) was a contribution of the structure of Ce_4O_7 (marked as □, JCPDS card 65-7999).

After increasing the O_2/Ar flow ratio to 0.25, the crystal structure of 20GDC films was transferred from the mixing oxidation state of cerium (Ce_2O_3, Ce_7O_{12} and Ce_4O_7) to the pure Ce_4O_7 structure. This result was similar, as seen with the XRD, to the results of 20GDC films which were deposited from a $Ce_{0.80}Gd_{0.20}O_{1.90}$ oxide target in the pure argon environment.[13] In raising the O_2/Ar flow ratio to 0.30, all the peaks belonging to Ce_4O_7 structure were shifted to the higher 2θ degree, revealing a well crystallized cubic fluorite structure of $Ce_{0.80}Gd_{0.20}O_{1.90}$ (marked as ▲, JCPDS card 75-0162) with <1 1 1> preferred orientation, indicating that there were no incomplete oxide materials in the 20GDC films at this O_2/Ar flow ratio.

3.4. Effect of chemical composition

From the XRD analysis results, the 20GDC films presented a mixing oxidation state of cerium at different O_2/Ar flow ratios, resulting in the distinct shifts in the binding energies for each valence state of cerium ions. Moreover, the characterization of multiple splitting of the $3d_{3/2}$ and $3d_{5/2}$ energy levels in Ce

3d region were also shown in the same spectrum which made it difficult to identify the contribution from each peak. Therefore, we imported the peak assignment from the work of Pfau and Schierbaum[25] in order to clarify the origin of the different structures, as shown in Table 1.

Fig. 5(a) was the high-resolution XPS spectrum in Ce 3d core levels of 20GDC films deposited at an O_2/Ar flow ratio of 0.05 after data processing. The characteristic peaks for the pure tetravalent states of Ce^{4+} binding states at 882.5 and 900.9 eV, 888.8 and 907.2 eV, and 916.7 eV are assigned as [$3d^0_{5/2}$ (v) and $3d^0_{3/2}$ (u)], [$3d^1_{5/2}$ (v″) and $3d^1_{3/2}$ (u″)] doublets, and [$3d^2_{3/2}$ (u‴)]. The characteristic peaks for the pure trivalent states of Ce^{3+} binding states at 884.7, 903.1 eV, and 881.0 eV are [$3d^2_{5/2}$ (v′) and $3d^2_{5/2}$ (u′)], and [$3d^0_{3/2}$ (v^0)]. The characteristic peaks for the mixing tetravalent and trivalent states of Ce^{4+} and Ce^{3+} binding states at 898.4 eV could be assigned as the overlapped result of [$3d^2_{3/2}$ (v‴)] and [$3d^0_{3/2}$ (u^0)]. After comparing the positions of binding energy for each peak, our data were well fitted in accordance with pure Ce_2O_3[15,18] and CeO_2 pellets[18]

Table 1
Initial states and final states of Ce^{3+} and Ce^{4+} ions in Ce 3d core level X-ray photoelectron spectroscopy spectra (v denotes the valance band, lines belonging to Ce $3d_{3/2}$ are labeled with u, lines belonging to Ce $3d_{5/2}$ are labeled with v)[25].

Ion	Initial state	Final state
Ce^{3+}	$3d^{10}4f^1$	v^0, u^0: $3d^94f^2V^{n-1}$
	$3d^{10}4f^1$	v′, u′: $3d^94f^1V^n$
Ce^{4+}	$3d^{10}4f^0$	v, u: $3d^94f^2V^{n-2}$
	$3d^{10}4f^0$	v″, u″: $3d^94f^1V^{n-1}$
	$3d^{10}4f^0$	v‴, u‴: $3d^94f^0V^n$

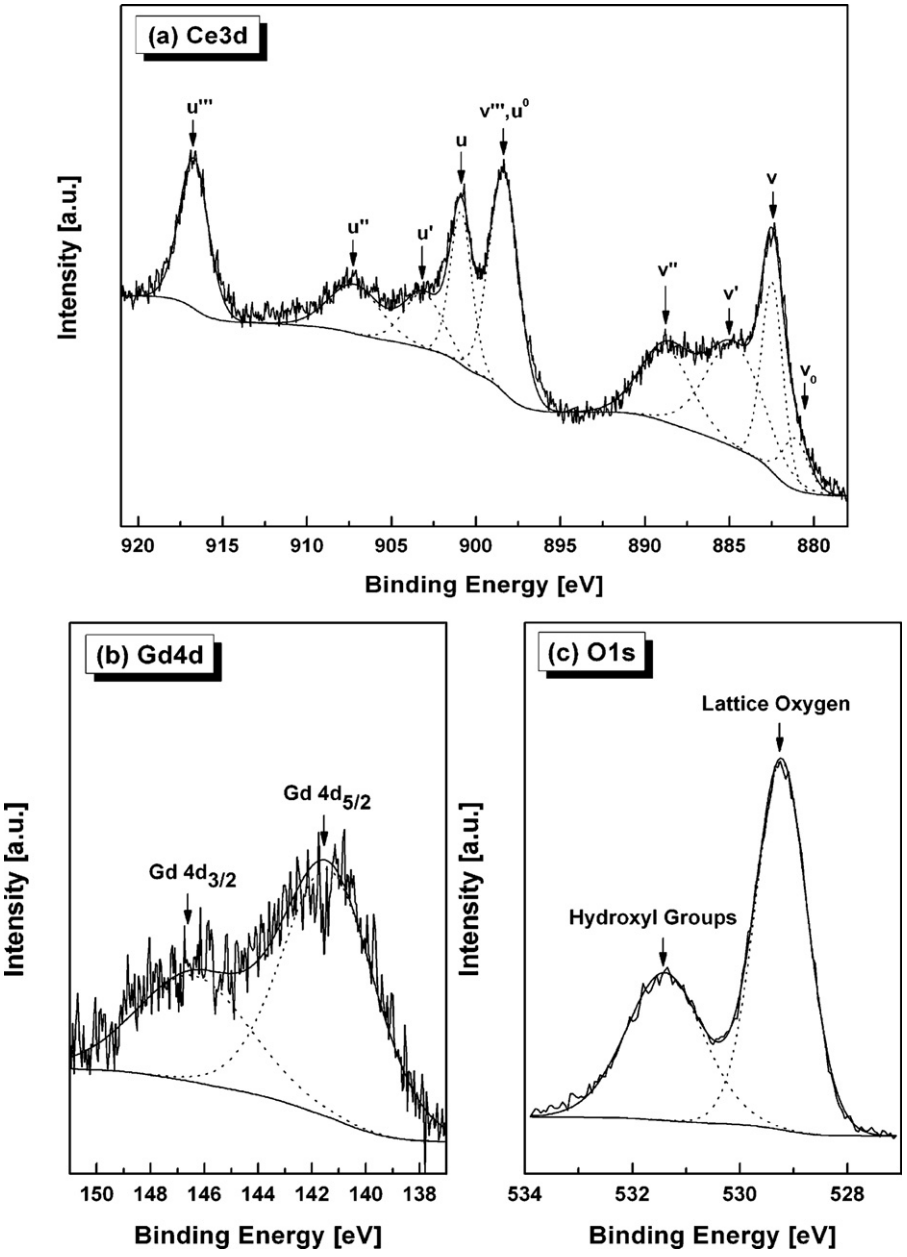

Fig. 5. XPS spectra of 20GDC films deposited at O_2/Ar flow ratio equals to 0.05 after data processing in (a) Ce 3d, (b) Gd 4d and (c) O 1s core levels.

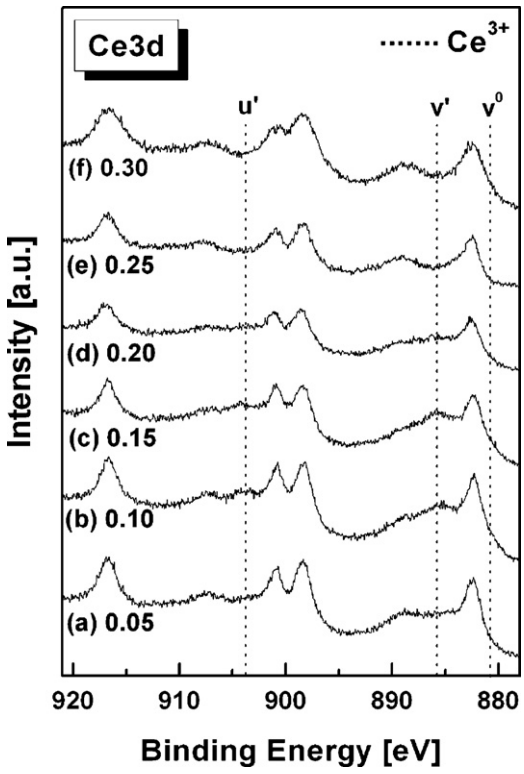

Fig. 6. Ce 3d core level spectra of 20GDC films deposited at various O_2/Ar flow ratios (a) 0.05, (b) 0.10, (c) 0.15, (d) 0.20, (e) 0.25 and (f) 0.30.

and $Ce_{0.80}Gd_{0.20}O_{1.90-x}$ films by spray pyrolysis[14] in the literature.

From examining the XPS spectra of Ce 3d core levels for 20GDC films deposited at different O_2/Ar flow ratios in Fig. 6, the peak intensities of Ce^{3+}-related [$3d^2_{5/2}$ (v′) and $3d^2_{5/2}$ (u′)] doublet are shown to increase gradually with increasing the O_2/Ar flow ratio until 0.15. They decrease gradually as the O_2/Ar flow ratio becomes higher than 0.15, then finally disappear at the O_2/Ar flow ratio of 0.30. These results imply that the amount of Ce^{3+} materials in the 20GDC films change with the increasing O_2/Ar flow ratios during sputtering deposition.

The amount of Ce^{3+} species in the 20GDC films for different O_2/Ar flow ratios can be adopted from the deconvolution results of Ce 3d core levels spectra by examining the amount of specific area for each peak. Table 2 represents the amount of specific area for each peak obtained at different O_2/Ar flow ratios after data processing. The peak area belonging to the Ce^{3+} related peaks (v′ and u′) was gradually increased and reached the maximum value at the O_2/Ar flow ratio of 0.15. It then decreased with increasing O_2/Ar flow ratios revealing a similar tendency to the observations of the varied intensities of Ce^{3+} related peaks described above.

Furthermore, the amount of Ce^{3+} species in the 20GDC films can also be estimated from the intensity of v’ and u’ lines, according to the following equation:[28]

$$Ce^{3+}\,(\%) = \frac{S_{v'} + S_{u'}}{(S_v + S_u)100\,(\%)}$$

where $S_{v'}$ and $S_{u'}$ are the intensities of v′ and u′ lines and S_v and S_u are the intensities of v and u lines.

These calculated results show that the amount of Ce^{3+} species in the as-deposited 20GDC films was around 40.55% for an O_2/Ar flow ratio of 0.05. This reached its highest value (64.43%) as the O_2/Ar flow ratio reached 0.15 and then decreased to zero as the O_2/Ar flow increased to 0.30. This conclusion was confirmed with our XRD data (Fig. 4) and assured that the diffraction peak, $2\theta = 30.00$, was the overlapped result of Ce and Ce_2O_3.

Fig. 5b presents the fitting result of Gd 4d core levels of 20GDC films deposited at O_2/Ar flow ratio equal to 0.05. The binding energies of Gd $4d_{3/2}$ and $4d_{5/2}$ in Fig. 6b, located at 146.39 eV and 141.39 eV, were the characteristic peaks of gadolinium oxide[14,17] and were without any significant change as with the 20GDC films prepared at different O_2/Ar flow ratios (not shown). Fig. 5c presents the results of O 1s core levels of 20GDC films deposited at O_2/Ar flow ratio equal to 0.05. Two contributions can be observed after data processing. The binding energy located at 529.23 eV was the photon electrons signal from a lattice oxygen of 20GDC films,[14] and the biding energy at 531.40 eV represents the hydroxyl groups directly bonded with the cerium atoms of films because of the high affinity of cerium atoms to hydroxyl groups.[26]

The chemical compositions of 20GDC films can be evaluated from the Ce 3d, Gd 4d, and O 1s peak areas corrected by appropriate sensitivity factors of $S_{Ce} = 7.399$, $S_{Gd} = 2.207$ and $S_O = 0.711$, respectively.[27] Fig. 7 displays the atomic ratio (O/(Ce + Gd)) of 20GDC films as a function of O_2/Ar flow ratio. While increasing the O_2/Ar flow ratio, the O/(Ce + Gd) ratio rose sharply and then became saturated around 2.05 for the O_2/Ar flow ratios over 0.25. The O/(Ce + Gd) ratio was larger than 1.90 for the expected result of $Ce_{0.80}Gd_{0.20}O_{1.90}$ when the O_2/Ar flow ratio was higher than 0.25. The excess amount of oxygen remaining in the 20GDC films can be explained by the higher oxygen partial pressure contributed from the O_2/Ar flow ratio over 0.25 during the sputtering process. The O_2/Ar flow ratio over 0.25 within the sputtering environment was in excess of the critical

Table 2
The comparisons of specific surface area for different energy states and the calculated amount of Ce^{3+} in Ce 3d core level at various O_2/Ar flow ratios.

O_2/Ar flow ratio	v^0	v	v′	v″	v‴, u^0	u	u′	u″	u‴	Total	Ce^{3+}%
0.05	1.90	19.34	12.24	9.53	18.15	11.29	7.43	6.65	13.47	100	40.55
0.10	3.71	17.27	15.06	8.42	16.27	10.12	10.69	6.01	12.45	100	55.95
0.15	4.76	15.82	16.55	8.16	15.97	9.55	11.93	5.83	11.42	100	64.43
0.20	2.95	18.63	14.11	8.17	17.01	10.1	9.33	5.82	13.87	100	49.53
0.25	1.03	20.70	8.15	10.62	22.77	11.27	3.06	7.05	15.36	100	22.18
0.30	0	25.4	0	11.96	25.35	13.07	0	7.73	16.48	100	0

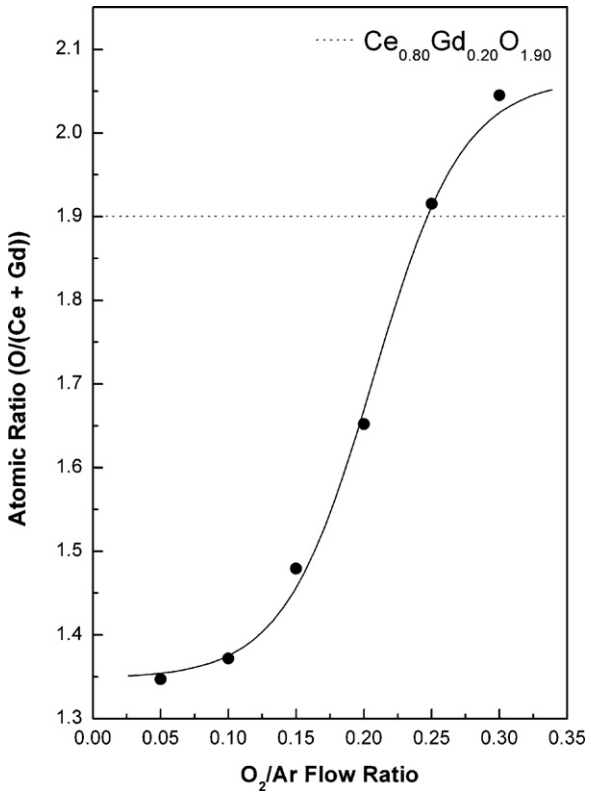

Fig. 7. Atomic ratio (O/(Ce + Gd)) of 20GDC films as a function of O_2/Ar flow ratio.

pressure, as mentioned before. The spare oxygen gases provided by the high oxygen partial pressure from the gas environment remained in the lattice structure or hid in the grain boundaries of 20GDC films during the sputtering deposition and subsequently resulted in the over-stoichiometry of 20GDC films for the O_2/Ar flow ratio over 0.25.

The XPS depth profile of the atomic composition for 20GDC films deposited at an O_2/Ar flow ratio of 0.15 is shown in Fig. 8. The spectrum includes data pertaining to cerium, gadolinium, oxygen, and carbon. Before inducing the Ar^+ ion sputtering on the film surface (sputtering time = 0 s), the carbon signals at 284.5 eV were detected largely due to a surface-bound layer of adventitious carbon. However, after sputtering during the first cycle (sputtering time = 120 s), the signals belonging to the adventitious carbon had disappeared leaving a pure 20GDC film surface with a chemical composition of $(Ce_{0.87}Gd_{0.13})O_{1.46}$ (Ce:Gd:O = 35.30:5.23:59.47). For the other sputter cycles, the chemical composition of 20GDC films remained at a constant value, revealing that the components of Ce, Gd and O are uniformly distributed throughout the bulk of the 20GDC films.

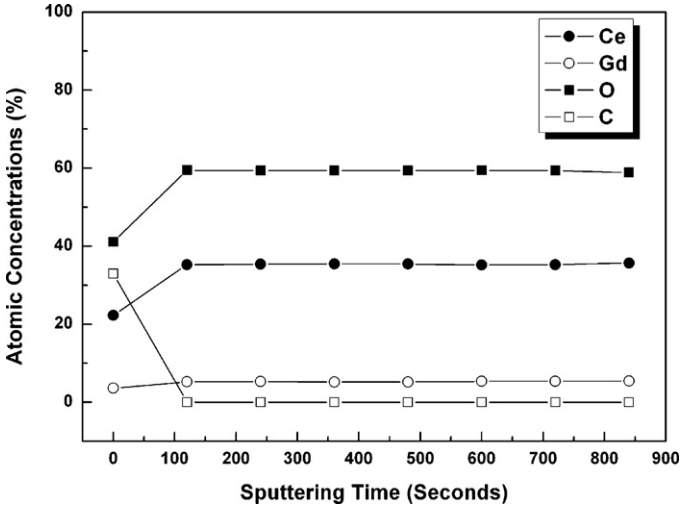

Fig. 8. XPS depth profile for 20GDC films deposited at an O_2/Ar flow ratio of 0.15.

Noticeably, the spectra of Ce 3d region showed a mixed oxidation state of cerium before inducing the Ar^+ ion sputtering on the 20GDC film surface, meaning that the Ce 3d valence band structure of ceria possessed a substoichiometric Ce^{4+}/Ce^{3+} condition. Nevertheless, after the first cycle of sputtering, the pure tetravalent states of Ce^{4+}-related uv doublets, u"v" doublets, and u‴ had disappeared and the pure trivalent states of Ce^{3+}-related u'v' doublets and v^0 were increased; the mixing tetravalent and trivalent states of Ce^{4+}- and Ce^{3+}-related v‴ and u^0 were also increased. This phenomenon has been documented and explained by other research groups,[20,21] showing that the valence state of ceria in 20GDC materials gradually reduces from Ce^{4+} to Ce^{3+} by being subjected to Ar^+ ion bombardment but with no change in its chemical composition based on the quantitative analysis of XPS results.[14]

For O 1s region, the lattice oxygen peak around 529.23 eV became stronger and the oxygen peaks ascribed to adsorbed hydroxyl groups around 531.40 eV were diminished by increasing the sputter time, whereas the Gd_2O_3 signals in the Gd 4d region showed no apparent change with regard to peak positions and amount.

4. Conclusions

This study investigated the deposition of 20 mol% Gd-doped ceria, 20GDC, thin films on alumina substrates using RF reactive sputtering from a cerium–gadolinium alloy target (80:20 at%) with various O_2/Ar flow ratios. Experiment results indicate that the deposition rate, surface morphology, crystal structure, and chemical composition of the 20GDC films depend on the O_2/Ar flow ratios. A stepwise change in deposition rate was observed at an O_2/Ar flow ratio of 0.25. The microstructure of 20GDC films were mainly composed of incompletely oxidized materials at lower O_2/Ar flow ratio, becoming a fully oxidized cubic fluorite structure as the ratio was increased to 0.30. As the O_2/Ar flow ratio increased, the O/(Ce + Gd) ratio increased steeply at first, and then become saturated at approximately 2.05 for O_2/Ar flow ratio over 0.25. The chemical composition of 20GDC films showed uniform distribution through the whole films for each O_2/Ar flow ratios.

As the incompletely oxidized materials (Ce_2O_3, Ce_7O_{12} and Ce_4O_7) remained in the as-deposited 20GDC films, a post-annealing treatment is needed in order to obtain fully oxidized $Ce_{0.80}Gd_{0.20}O_{1.90}$ materials, a process now under investigation. The electricity conductivity behavior of O_2/Ar flow ratios and

the annealing temperature effects of reactive sputtered 20GDC films are also under investigating in the following project.

Acknowledgements

The authors would like to thank the National Science Council of the Republic of China for financially supporting this research under contract no. NSC 96-2218-E-036-002 and NSC 99-2221-E-011-121-MY2.

References

1. Yahiro H, Ohuchi T, Eguchi K, Arai H. Electrical properties and microstructure in the system ceria–alkaline earth oxide. *J Mater Sci* 1988;**23**: 1036–41.
2. Yahiro H, Eguchi K, Arai H. Electrical properties and reducibility of ceria–rare earth oxide systems and their application to solid oxide fuel cell. *Solid State Ionics* 1989;**36**:71–5.
3. Eguchi K, Setoguchi T, Inoue T, Arai H. Electrical properties of ceria-based oxides and their application to solid oxide fuel cells. *Solid State Ionics* 1992;**52**:165–72.
4. Steele BCH. Appraisal of $Ce_{1-y}Gd_yO_{2-y/2}$ electrolytes for IT-SOFC operation at 500 °C. *Solid State Ionics* 2000;**129**:95–110.
5. Steele BCH, Heinzel A. Materials for fuel-cell technologies. *Nature* 2001;**414**:345–52.
6. Pan M, Meng GY, Xin HW, Chen CS, Peng DK, Lin YS. Pure and doped CeO_2 thin films prepared by MOCVD process. *Thin Solid Films* 1998;**324**:89–93.
7. Song HZ, Wang HB, Zha SW, Peng DK, Meng GY. Aerosol-assisted MOCVD growth of Gd_2O_3-doped CeO_2 thin SOFC electrolyte film on anode substrate. *Solid State Ionics* 2003;**156**:249–54.
8. Laukaitis G, Dudonis J, Milcius D. Properties of YSZ thin films deposited by e-beam technique. *Solid State Ionics* 2008;**179**:182–7.
9. Wang LS, Thiele ES, Barnett SA. Sputter deposition of yttria-stabilized zirconia and silver cermet electrodes for SOFC applications. *Solid State Ionics* 1992;**52**:261–7.
10. Kuo YL, Lee C, Chen YS, Liang H. Gadolinia-doped ceria films deposited by RF reactive magnetron sputtering. *Solid State Ionics* 2009;**180**: 1421–8.
11. Nagata A, Okayama H. Characterization of solid oxide fuel cell device having a three-layer film structure grown by RF magnetron sputtering. *Vacuum* 2002;**66**:523–9.
12. Yoo Y. Fabrication and characterization of thin film electrolytes deposited by RF magnetron sputtering for low temperature solid oxide fuel cells. *J Power Sources* 2006;**160**:202–6.
13. Lin SE, Kuo YL, Chou CH, Wei WC. Characterization of electrolyte films deposited by using RF magnetron sputtering a 20 mol% gadolinia-doped ceria target. *Thin Solid Films* 2010;**518**:7229–32.
14. Rupp JLM, Drobek T, Rossi A, Gauckler LJ. Chemical analysis of spray pyrolysis gadolinia-doped ceria electrolyte thin films for solid oxide fuel cells. *Chem Mater* 2007;**19**:1134–42.
15. Rao MVR, Shripathi T. Photoelectron spectroscopic study of X-ray induced reduction of CeO_2. *J Electron Spectrosc Related Phenom* 1997;**87**:121–6.
16. Paparazzo E. XPS studies of damage induced by X-ray irradiation on CeO_2 surfaces. *Surf Sci Lett* 1990;**234**. L253-8.
17. Terzieff P, Lee K. Electron spectroscopy studies on amorphous GdFe and GdCo alloys. *J Appl Phys* 1979;**50**:3565–9.
18. Uwamino Y, Ishizuka T. X-ray photoelectron spectroscopy of rare-earth compounds. *J Electron Spectrosc Related Phenom* 1984;**34**:67–8.
19. Briggs D, Seah MP. *Practical Surface Analysis*. New York: John Wiley & Sons; 1990.
20. Holgado JP, Alvarez R, Munuera G. Study of CeO_2 XPS spectra by factor analysis: reduction of CeO_2. *Appl Surf Sci* 2000;**161**:301–15.
21. Qiu L, Liu F, Zhao L, Ma Y, Yao J. Comparative XPS study of surface reduction for nanocrystalline and microcrystalline ceria powder. *Appl Surf Sci* 2006;**252**:4931–5.
22. Kuo YL, Lee C, Lin JC, Peng CH, Chen LC, Hsieh CH, et al. Growth of (Ti,Zr)N films on Si by DC reactive sputtering of TiZr in N_2/Ar gas mixtures: effect of flow ratio. *J Electrochem Soc* 2004;**151**:C176–81.
23. Mayrhofer F PH, Tischler G, Mitterer C. Microstructure and mechanical/thermal properties of Cr–N coatings deposited by reactive unbalanced magnetron sputtering. *Surf Coat Technol* 2001;**142–144**:78–84.
24. Zhou J, Wu Z, Liu Z. Influence and determinative factors of ion-to-atom arrival ratio in unbalanced magnetron sputtering systems. *J Univ Sci Technol B* 2008;**15**:775–81.
25. Pfau A, Schierbaum KD. The electronic structure of stoichiometric and reduced CeO_2 surfaces: an XPS, UPS and HREELS study. *Surf Sci* 1994;**321**:71–80.
26. Borchert H, Frolova YV, Kaichev VV, Prosvirin IP, Alikina GM, Lukashevich AI, et al. Electronic and chemical properties of nanostructured cerium dioxide doped with praseodymium. *J Phys Chem B* 2005;**109**:5728–38.
27. Moulder JF, Stickle WF, Sobol PE, Bomben KD. *Handbook of X-ray Photoelectron Spectroscopy*. Minnesota: Physical Electronics, Inc.; 1995.
28. Francisco MSP, Mastelaro VR, Nascente PAP, Florentino AO. Activity and characterization by XPS, HR-TEM, Raman spectroscopy, and BET surface area of CuO/CeO_2–TiO_2 catalysts. *J Phys Chem B* 2001;**105**:10515–22.